Journal of Catalysis 261 (2009) 116–128

Contents lists available at ScienceDirect

Journal of Catalysis

www.elsevier.com/locate/jcat

The nature of active chromium species in Cr-catalysts for dehydrogenation of propane: New insights by a comprehensive spectroscopic study

M. Santhosh Kumar [a,*,1], Nina Hammer [a], Magnus Rønning [a], Anders Holmen [a,*], De Chen [a], John C. Walmsley [b,c], Gisle Øye [d]

[a] Department of Chemical Engineering, Norwegian University of Science and Technology (NTNU), N-7491 Trondheim, Norway
[b] Department of Physics, Norwegian University of Science and Technology (NTNU), N-7491 Trondheim, Norway
[c] SINTEF Materials and Chemistry, N-7465 Trondheim, Norway
[d] Ugelstad Laboratory, Norwegian University of Science and Technology (NTNU), N-7491 Trondheim, Norway

ARTICLE INFO

Article history:
Received 18 September 2008
Revised 16 November 2008
Accepted 21 November 2008
Available online 4 December 2008

Keywords:
Propane dehydrogenation
Cr–SBA-15
Cr–Al_2O_3
XRD
UV-Raman spectroscopy
STEM
In situ XAS
Isolated Cr sites
Oligomeric Cr species
Active sites

ABSTRACT

Dehydrogenation of propane (DHP) was studied over a series of *x*Cr–SBA-15 and *x*Cr–Al_2O_3 catalysts, prepared by incipient wetness impregnation, to gain a better understanding of the nature and distribution of Cr species and their catalytic function. To this end, the catalysts were characterized by N_2-physisorption, X-ray diffraction (XRD), UV-Raman spectroscopy, scanning transmission electron microscopy–energy dispersive X-ray spectroscopy (STEM–EDXS) and X-ray absorption spectroscopy (XANES and EXAFS). All these characterization techniques indicate that, at $\leqslant$1 wt% Cr, SBA-15 contains exclusively uniform distribution of chromium as isolated Cr(VI) species in tetrahedral (T_d) coordination, whilst on γ-Al_2O_3 a fraction of oligomers (including dimers) is present along with isolated species. At $\geqslant$5 wt% Cr, SBA-15 is dominated by crystalline α-Cr_2O_3 particles, besides a fraction of isolated Cr(VI) species in T_d coordination. Remarkably, γ-Al_2O_3 contains mainly oligomers with different degrees of nuclearity and a fraction of isolated species but no Cr_2O_3 particles. Among *x*Cr–SBA-15 catalysts, those containing exclusively isolated Cr species (i.e., $\leqslant$1 wt% Cr) exhibit higher activity and selectivity with respect to per mole of Cr than the catalyst dominated by crystalline α-Cr_2O_3 particles ($\geqslant$5 wt% Cr). The intrinsic activity of these isolated Cr species is higher than those observed on γ-Al_2O_3 ($\leqslant$1 wt% Cr). Interestingly, among *x*Cr–Al_2O_3, the catalysts dominated by oligomeric species show the highest activity, indicating the important role of the species in the reaction. In situ XAS studies evidence that active Cr sites are apparently generated on-site during the reaction and that Cr is typically in (III) oxidation state. Based on ex situ and in situ characterization results and catalytic data, it appears that the activity of the Cr species is different in *x*Cr–SBA-15 and *x*Cr–Al_2O_3. For *x*Cr–SBA-15, isolated Cr(III) sites with coordination number greater than four are more active, selective and stable than Cr sites on the surface of crystalline Cr_2O_3. In contrast, for *x*Cr–Al_2O_3, oligomeric Cr species are more active and selective than the isolated Cr sites.

1. Introduction

Dehydrogenation of propane (DHP) is one of the on-purpose propylene production technologies that has received much attention in the recent past [1,2] due to it's potential to make-up the shortfall of propylene supply left by conventional crackers (e.g., FCC) [3–5]. Propylene is an important building block in a myriad of (petro)chemical applications, for instance in the production of polypropylene [6,7]. Typically, the CrO_x–Al_2O_3 catalyst system is used for industrial processes, for example in the Catofin process (ABB Lummus) that runs at cyclic operation (reaction and regeneration) at ~850 K [8]. However, major challenges associated with this catalytic system are cracking and coking which influence the product selectivity and catalyst stability, respectively. Thus, the deactivated catalyst must frequently be regenerated without losing dehydrogenation activity, selectivity to propylene and catalyst stability, which makes the process not only complex but also expensive. Therefore, considerable research has been done to gain a deep fundamental knowledge on the structure–reactivity relationships of Cr catalysts in dehydrogenation of alkanes by various characterization techniques [9–18] and to improve catalytic performance.

* Corresponding authors. Fax: +41 44 823 4041.
E-mail addresses: santhosh.matam@empa.ch (M. Santhosh Kumar), anders.holmen@chemeng.ntnu.no (A. Holmen).
[1] Present address: Laboratory for Solid State Chemistry and Catalysis, Eidgenössische Materialprüfungs und Forschungsanstalt (EMPA), CH-8600 Dübendorf, Zürich, Switzerland.

0021-9517/$ – see front matter
doi:10.1016/j.jcat.2008.11.014

Alternatively, oxidative dehydrogenation of propane (ODHP) was also extensively studied to overcome the challenges associated with DHP however without much success in terms of commercial viability [19]. Nonetheless, CO_2 was interestingly reported as an alternative to O_2 or N_2O as an oxidizing agent for ODHP, in which again Cr based catalysts were found to be more active than other metal catalysts [16,20–22]. Especially, Cr supported on silicon (either on SiO_2 or on siliceous mesoporous materials like SBA-15 and MCM-41) have shown higher activity than the regular catalysts, for example on Al_2O_3 [20,21]. Thus, these materials have recently got attention to understand their better catalytic performance either in ODHP or in DHP as compared to other catalysts [15,16,20].

As evidenced from various studies, the distribution of Cr species is strongly dependent on the nature of the support, Cr content and method of activation [23–30]. A variety of Cr species (isolated, dimers, trimers, polymeric species with different nuclearity and large Cr_2O_3 clusters) with different oxidation and coordination states and with different redox properties coexist in the same catalyst. It is known that DHP activity increases with Cr loading and a typical industrial Cr catalyst contains ~13 wt% Cr at which level heterogeneous distribution of Cr species is virtually unavoidable [23–30]. Thus, it has been a major challenge to gain definitive information on the nature of active Cr sites. As a result, the nature of active Cr species in Cr catalysts during DHP remains elusive and is still a subject of debate [9–18]. For instance, studies on Cr–ZrO_2 catalysts with a Cr content of 0.05 to 0.8 wt% showed that mononuclear Cr(III) species are the active sites [31]. The same conclusion was also reached after considerable studies on Cr–Al_2O_3 and other Cr catalysts [13,32–34]. In contrast, it was concluded that coordinatively unsaturated clustered Cr(III) and/or Cr(II) sites play an important role in the activation of alkanes while crystalline α-Cr_2O_3 are rather inert [9,10,12]. In a different study, La doped Cr–Al_2O_3 and Cr–ZrO_2 catalysts monitored during DHP simultaneously by in situ—EPR and—UV/vis coupled with online GC showed that in both the catalysts the oxidation state of Cr is not higher than (III) however, coordination state of Cr species was not discussed [11]. The structure of Cr species in differently prepared Cr–MCM-41 (Cr content varied between 0.35 and 1.7 wt%) studied by in situ XAS (XANES and EXAFS) showed that aggregated Cr(III) are the active sites for DHP [15,16], which is similar to that concluded on Cr–Al_2O_3 [12]. On the other hand, a study on the oxidative dehydrogenation of ethane (ODHE) with CO_2 over Cr/H-ZSM-5 concludes that a redox cycle between Cr^{+6} and Cr^{+3} is important for a high dehydrogenation rate [22].

In the present work, a series of Cr catalysts with varying Cr content (0.5–10 wt%) was prepared aiming to create a well defined Cr site distribution in the catalysts and thereby to derive the catalytic function of each specific Cr species. To this end, SBA-15 and γ-Al_2O_3 supports were employed. On high surface area mesoporous SBA-15, it was expected that highly dispersed and completely accessible isolated Cr species can be created. The large pores and the weak acidity of SBA-15 should facilitate adequate transport of gaseous reactants and products to and from the active Cr species. This in turn should lead to better catalytic performance and stability than the regular catalysts [20]. The structure and catalytic properties of these Cr species are compared with those supported on γ-Al_2O_3, which is typically used in industrial DHP processes and is also known to contain well defined Cr site distribution depending on the Cr content [26,27,30]. This will allow us to investigate the influence of the molecular structure, which is dependent on the nature of the support as evident from literature, of Cr species on DHP with identical Cr content and in some cases (at $\leqslant$1 wt% Cr) with similar Cr distribution. The nature and distribution of Cr species in the catalysts was thoroughly investigated by various characterization techniques that are complementary to each other. The behavior of Cr species during DHP was monitored by in situ—X-ray absorption spectroscopy (XAS) which is a powerful tool to investigate the oxidation and coordination state of Cr species, however under suitable experimental conditions [36]. Steady-state catalytic activity tests were performed isothermally at 853 K. The correlation of steady-state activity data and characterization results derived from ex situ and in situ spectroscopic studies enabled us to gain new insights into the nature of active Cr species involved in DHP.

Table 1
Chemical composition and textural properties of the catalysts.

Catalyst	Cr[a] (wt%)	V_{total}[b] ($cm^3\,g^{-1}$)	S_{BET}[c] ($m^2\,g^{-1}$)	Pore size[b] (nm)
0.5Cr–SBA-15	0.5	1.11	535	7.7
1Cr–SBA-15	1.0	1.13	532	7.7
5Cr–SBA-15	5.0	1.03	485	7.7
10Cr–SBA-15	10	0.95	445	7.8
0.5Cr–Al_2O_3	0.5	0.39	174	7.7
1Cr–Al_2O_3	1.0	0.35	152	7.1
5Cr–Al_2O_3	5.0	0.34	150	5.7/7.65
10Cr–Al_2O_3	10	0.28	140	5.5

[a] Nominal loading.
[b] BJH method.
[c] BET method.

2. Experimental

2.1. Preparation of catalysts

The parent siliceous SBA-15 was prepared in our laboratory according to the recipe reported elsewhere [37–39]. Briefly, a gel prepared from Pluronic P123 ($EO_{20}PO_{70}EO_{20}$, BASF), the template, 2 M HCl and tetraethylorthosilicate (TEOS, Alfa Aesar, 99%), silicon source, was stirred at 313 K for 24 h. The gel was then transferred into a Teflon bottle and aged in an oven at 373 K for 48 h. The resulting white solid was filtered, washed thoroughly with double deionized water and dried at room temperature for 24 h. The final product was then calcined in flowing air at 823 K for 6 h to remove the template and thereby to produce mesoporous SBA-15. The γ-Al_2O_3 (Puralox from Sasol) was calcined at 773 K for 6 h prior to using it as a catalyst support.

A series of *x*Cr–SBA-15 and *x*Cr–Al_2O_3 catalysts (*x* in the catalyst label represents the nominal Cr content, wt%) were prepared by incipient wetness impregnation. Impregnation solutions were prepared by dissolving appropriate amounts of $Cr(NO_3)_2\,9H_2O$ (Merck, 98–100%) in double deionized water. The resulting solution was added dropwise to the supports, which have been pre-treated in an oven at 373 K for 16 h. After impregnation, the samples were dried at 383 K for 10 h and subsequently calcined at 823 K for 5 h, with a heating rate of 2 $K\,min^{-1}$. Physical appearances of the catalysts are as follows: 0.5Cr–SBA-15 and 1Cr–SBA-15 are pale yellow while 5Cr–SBA-15 and 10Cr–SBA-15 are dark green which is characteristic of the reference sample α-Cr_2O_3. Interestingly, none of the catalysts in the series of *x*Cr–Al_2O_3 show the latter color and 0.5Cr–Al_2O_3 is the only one that is pale yellow. 1Cr–Al_2O_3 is pale yellow with a shade of pale green. 5Cr–Al_2O_3 and 10Cr–Al_2O_3 are light and dark brownish in color, respectively. The varying colours of the catalysts indicate that Cr speciation is different in them [22]. The composition and textural properties of the catalysts are presented in Table 1.

2.2. Characterization techniques

Nitrogen adsorption and desorption isotherms at 77 K were obtained on a Micromeritics TriStar 3000 instrument. Prior to the experiments, the samples were evacuated at 473 K for 12 h. The total surface area of the samples was determined by the Brunauer–Emmett–Teller (BET) method. The pore size distributions were

obtained from the desorption branch of the isotherm using the Barrett–Joyner–Halender (BJH) model [40].

The powder X-ray diffraction (XRD) patterns of the catalysts were collected on a D8FOCUS (Bruker AXS) instrument using CuKα radiation ($\lambda = 1.54$ Å, 35 kV and 40 mA). XRD data were collected in the 2θ range of 20°–80° using a step size of 0.020° and a step time of 2.5 s.

Scanning transmission electron microscopy (STEM) and energy dispersive X-ray spectroscopy (EDXS) measurements were performed using a JEOL 2010F microscope operated at 200 kV. The catalysts were dispersed in isopropanol and dropped on carbon-film coated copper grids and dried in air.

UV-Raman measurements were performed on a LabRam HR-UV spectrometer (Horiba Jobin Yvon). The spectra were recorded with a 325 excitation laser provided by He–Cd source. Spectra were recorded at an exposure time of 10 s and an accumulation number of 20.

X-ray absorption spectroscopy (XAS) data were collected in transmission mode at the Swiss–Norwegian Beamlines (SNBL) at the European Synchrotron Radiation Facility (ESRF), Grenoble. Spectra were obtained at the Cr K-edge (5.989 keV) using a double crystal Si(111) monochromator and higher order harmonics were rejected by detuning the crystals. Ion chamber detectors were used to determine intensities of the incident (I_o) and transmitted (I_t) X-rays. Based on the Cr content in the catalysts, required amounts of catalyst powder were mixed with desired amounts of boron nitride (BN) to obtain an appropriate absorber thickness. In situ XAS experiments were carried out in a heatable X-ray reaction cell equipped with a temperature programmer and a gas-dosing system with mass-flow controllers. In situ experiments were performed at 823 K according to the following sequence: (a) oxidative pretreatment in 5% O_2 in He (15 ml min^{-1}) for 1 h, (b) behavior of Cr species during DHP is studied by changing the flow from O_2 to 5% C_3H_8 in He (15 ml min^{-1}) for 15 min (denoted as first run), (c) followed by regeneration by switching to 5% O_2 in He (15 ml min^{-1}) and (d) subsequently a second DHP run was performed by changing the flow from O_2 to 5% C_3H_8 in He (15 ml min^{-1}) for 1 h. After every step, the catalyst was flushed with He flow for 5 min. After step (d), the catalyst was cooled down to room temperature in the flow of He and the extended X-ray absorption fine structure (EXAFS) spectra were then recorded. In the first run, in situ X-ray absorption near edge structure (XANES) spectra were recorded during DHP at 823 K in the following intervals by switching flow from C_3H_8 to pure He: after 90 s and at every 3, 10 and 15 min. In the second run, XANES spectra were taken before (i.e., after the regeneration) and after 1 h DHP at 823 K as well as at room temperature after cooling down in the flow of He.

The *WINXAS* v3.1 software was used for XANES analysis to obtain qualitative and quantitative information on Cr species [41]. The XAS data were pre-edge background subtracted (linear fit) and normalized. The EXAFS data were treated with the program *EXCURV98* using curved-wave theory and *ab initio* phase shifts [42]. Chromium metal foil, CrO_2, CrO_3, Cr_2O_3, Na_2CrO_4, $K_2Cr_2O_7$, chromium acetate and $CrCl_3$ were used as model compounds. The XANES spectra of the model compounds were used to assess the different chromium phases that are present in the catalysts by a linear combination method.

The catalysts performance in the DHP reaction was studied using a tapered element oscillating microreactor (TEOM, Series 1500 PMA, Rupprecht and Patashnick Co.) that is connected to an online gas-chromatograph (GC), which is a well established system in our laboratory for this reaction. Moreover, a TEOM reactor was also recently used by other researchers to investigate the feasibility of a cyclically operated continuous propylene production process via oxidative dehydrogenation of propane with N_2O on Fe-zeolites [43]. However, in the present study the mass change due to coke formation could not be measured because of a high noise level. The detailed description of the equipment employed in the present study was reported elsewhere [1,39]. Gas flows, temperatures, TEOM operation and data collection were controlled and operated using Lab-View software.

The TEOM reactor was loaded with 50 mg of catalyst, firmly packed between two plugs of quartz wool and retained there by a ventilated metal cap [1,39]. Prior to the experiments, the catalysts were pre-treated in flowing O_2 (5 ml min^{-1} in 45 ml min^{-1} of He) at 753 K for 1 h followed by heating in He flow (50 ml min^{-1}) to the reaction temperature (853 K). At this temperature, DHP (5 ml min^{-1} of C_3H_8 in 45 ml min^{-1} of He) was carried out for 2 h (denoted as first run). Afterwards, the catalyst was cooled down to 753 K in a flow of He and regenerated by replacing He flow with O_2 (5 ml min^{-1} in 45 ml min^{-1} of He) for 1 h. Subsequently by changing the flow from O_2 to He (50 ml min^{-1}), the catalyst was heated to the reaction temperature where a second DHP run was performed to investigate the influence of the regeneration step on the catalytic activity. The gaseous reaction mixture was preheated at 723 K in the preheating zone before entering on to the catalyst bed. A purge gas (He) flow of 200 ml min^{-1} was used. The space velocity (SV) was calculated as $g_{propane}\, g_{cat}^{-1}\, h^{-1}$ and was 11.78 h^{-1}. The product gases were analyzed by an online GC (HP 5890) equipped with a FID, using GS-Q column (30 m length and 0.543 mm i.d., allowing the separation of hydrocarbons upto C_3) and controlled by HP ChemStation software. The conversion of propane was calculated from the amount (in mole fraction) of propane detected at the outlet by GC. The selectivity of the product was calculated from the amount of the product formed divided by the amount of propane reacted.

3. Results and discussion

3.1. Characterization of catalysts

3.1.1. N_2 adsorption–desorption

The chemical composition and textural properties of the catalysts are compared in Table 1. The N_2 adsorption–desorption isotherms and pore size distribution of Cr supported SBA-15 are shown in Fig. 1. The isotherms of the catalysts show the characteristic behavior of ordered mesoporous materials exhibiting an irreversible type IV isotherm with a well-defined hysteresis loop of type H1 at $p/p_0 > 0.66$ (Fig. 1A), which can be associated with capillary condensation and desorption in open ended cylindrical mesopores [38,44]. The pore diameter distribution in the catalysts was determined by the BdB model applied to the desorption branch of the isotherms. It predicts a pore size distribution between 7.2–8.3 nm in the catalysts (Fig. 1B). The total BET surface area and pore volume of the catalysts are decreasing, as expected, with increasing Cr content. This suggests that at higher Cr loadings some of the pores might be partly occupied by chromium (Table 1). However, N_2 adsorption–desorption isotherms of the catalysts and the pore size distribution in them (Fig. 1 and Table 1) clearly show that the mesoporous structure is not disrupted even at the highest Cr content in the catalyst.

Fig. 2 shows N_2 adsorption–desorption isotherms and pore size distribution of Cr supported on γ-Al_2O_3 catalysts. Like *x*Cr–SBA-15, the isotherms of these catalysts also represent the type IV with a hysteresis loop of type H1, indicating the presence of mesopores [45,46]. The catalysts with $\leqslant$1 wt% Cr exhibit a well-defined hysteresis loop at $p/p_0 > 0.66$ while, it shifted to the left (at $p/p_0 > 0.56$) for the catalysts with $\geqslant$5 wt% Cr (Fig. 2A), suggesting a partial coverage of pores by Cr species. This is also reflected in the pore size distribution in the catalysts (Fig. 2B). It can be seen from Fig. 2B and Table 1 that catalysts with $\leqslant$1 wt% Cr show an average pore diameter of ~7 nm while, the 5Cr–Al_2O_3 exhibits a

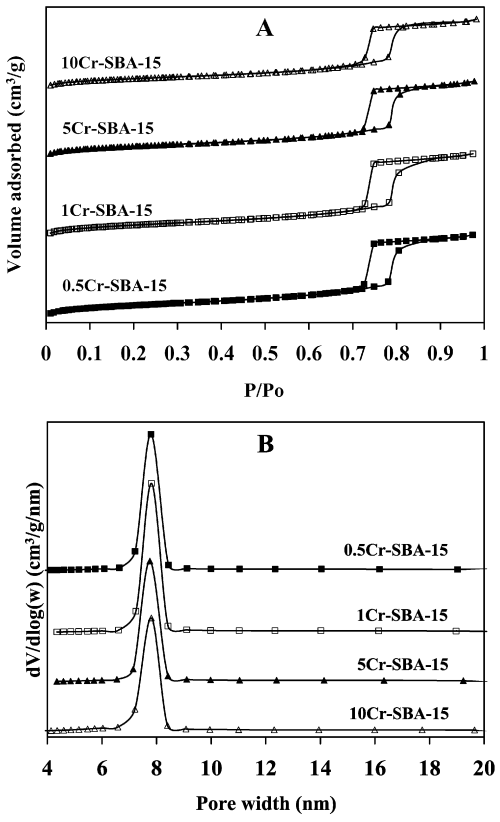

Fig. 1. N_2 adsorption–desorption isotherms of the catalysts (A) and the corresponding pore size distribution as obtained from the desorption branch (B).

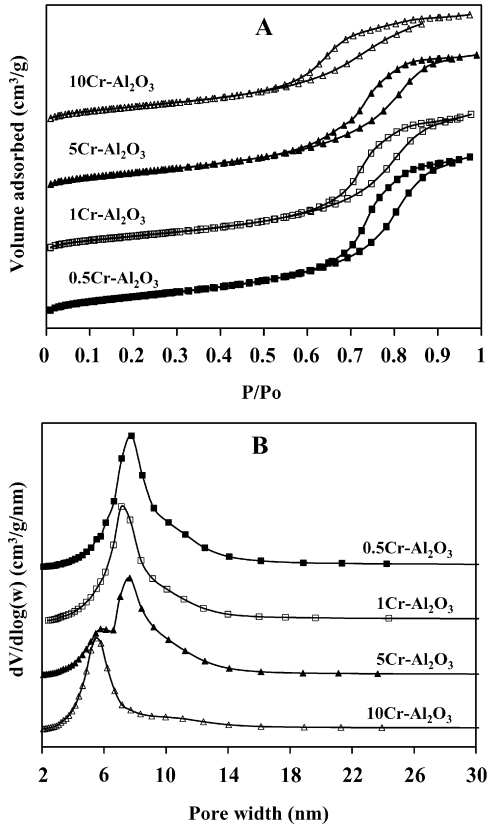

Fig. 2. N_2 adsorption–desorption isotherms of the catalysts (A) and the corresponding pore size distribution as obtained from the desorption branch (B).

bimodal pore size distribution indicating the presence of Cr species within the pores. Accordingly, by increasing the Cr content from 5 to 10 wt% in 10Cr–Al_2O_3, a distribution of an uniform pore size of ~5 nm was achieved. Such behavior was not observed for support SBA-15 and it indicates that Cr species are essentially located within the pore of Al_2O_3 with perhaps uniform distribution.

3.1.2. X-ray diffraction

XRD patterns of the catalysts are compared in Fig. 3. Catalysts 5Cr–SBA-15 and 10Cr–SBA-15 show XRD reflections at 2θ of 24.6°, 33.2°, 36.2°, 41.6°, 50.3°, 54.9°, 63.5°, 65.15°, 73.05° and 76.87° which are characteristic for crystalline α-Cr_2O_3 phase [36,47,48]. These XRD reflections are not observed for catalysts 0.5Cr–SBA-15 and 1Cr–SBA-15. Similarly, the series of xCr–Al_2O_3 show XRD reflections of the support but no reflections that can be assignable to chromium oxide phases, indicating that either chromium is highly dispersed in the catalysts or that the size of Cr_xO_y clusters may be small to be detected by XRD. Therefore, the catalysts were further characterized by STEM and EDXS.

3.1.3. STEM and EDXS

STEM and EDXS were used to investigate the morphology of the support materials and distribution of Cr species as well as the degree of agglomeration of chromium oxide species (Fig. 4A). It should be mentioned that analysis for 1 and 5 wt% Cr catalysts are presented assuming that they would also represent 0.5 and 10 wt% Cr catalysts, respectively. In Fig. 4, it is seen that support SBA-15 particles show the characteristic rod-like morphology with more or less uniform size distribution [37]. The morphology of both the support materials is intact even after Cr deposition followed by subsequent pre-treatments. For instance, the well ordered uniform mesoporous channels of support SBA-15 can be seen the micrographs in regions where the sample is suitable oriented. The STEM micrographs of 1Cr–SBA-15, 1Cr–Al_2O_3 and 5Cr–Al_2O_3 in Fig. 4A do not show any clusters of Cr_xO_y species indicating that Cr is well dispersed within the pores of the support, while 5Cr–SBA-15 contains crystalline Cr_2O_3 particles which can be seen as bright essentially needle-shaped and a few cube-shaped structures, in agreement with XRD. The size of the crystals is much larger than the size of pores in the support SBA-15 (Table 1). Thus, it can be suggested that the crystals are located at the external surface of SBA-15. EDXS confirms on the one hand the formation of crystalline Cr_2O_3 particles in 5Cr–SBA-15 and on the other hand the uniform distribution of Cr species within the pores of the catalyst 5Cr–Al_2O_3 (Fig. 4B). To assess this, the catalysts were further characterized by UV-Raman spectroscopy which provides molecular information on the state of Cr species in the catalysts.

3.1.4. UV-Raman spectroscopy

UV-Raman spectra of the series of xCr–SBA-15 and xCr–Al_2O_3 are shown in Fig. 5. It can be readily seen that the position and shape of Raman bands are different for both types of catalysts indicating that the molecular structure of Cr species might be different. Raman bands, in particular in the range from 800 to 1000 cm^{-1}, are narrow and more defined in the spectra of xCr–SBA-15 whereas, for xCr–Al_2O_3 they are broad and several bands overlap. Nonetheless, the catalysts show characteristic Raman bands of chromium oxo species that are similar to the previous observations reported on Cr supported on SiO_2 and Al_2O_3 [23–30]. Despite extensive studies on the supported chromium catalysts by Raman spectroscopy, the assignment of Raman bands is not straightforward [16,24–30,49], which could be due to the complex nature of the catalytic system.

As seen in Fig. 5a, 0.5Cr–SBA-15 shows an intense and narrow band at ~982 cm^{-1} which is frequently assigned to symmetric stretching of Cr=O of surface monochromate species (CrO_4^{2-}). Additionally, less intense and broad chromium oxo Raman bands are

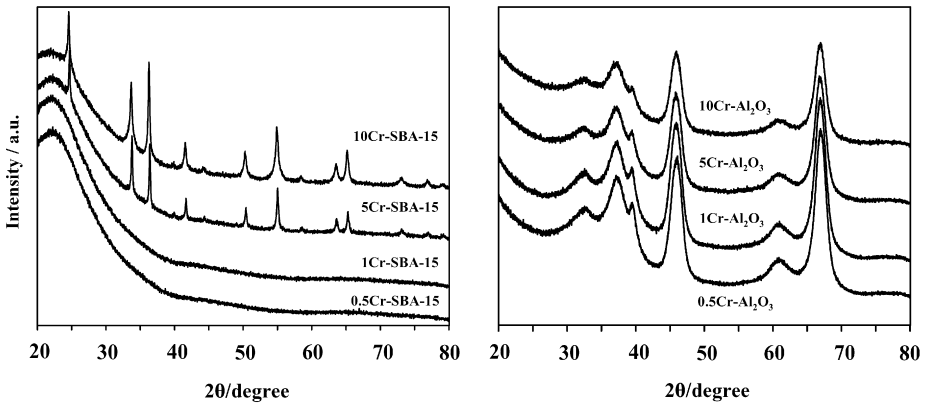

Fig. 3. XRD powder patterns of the catalysts.

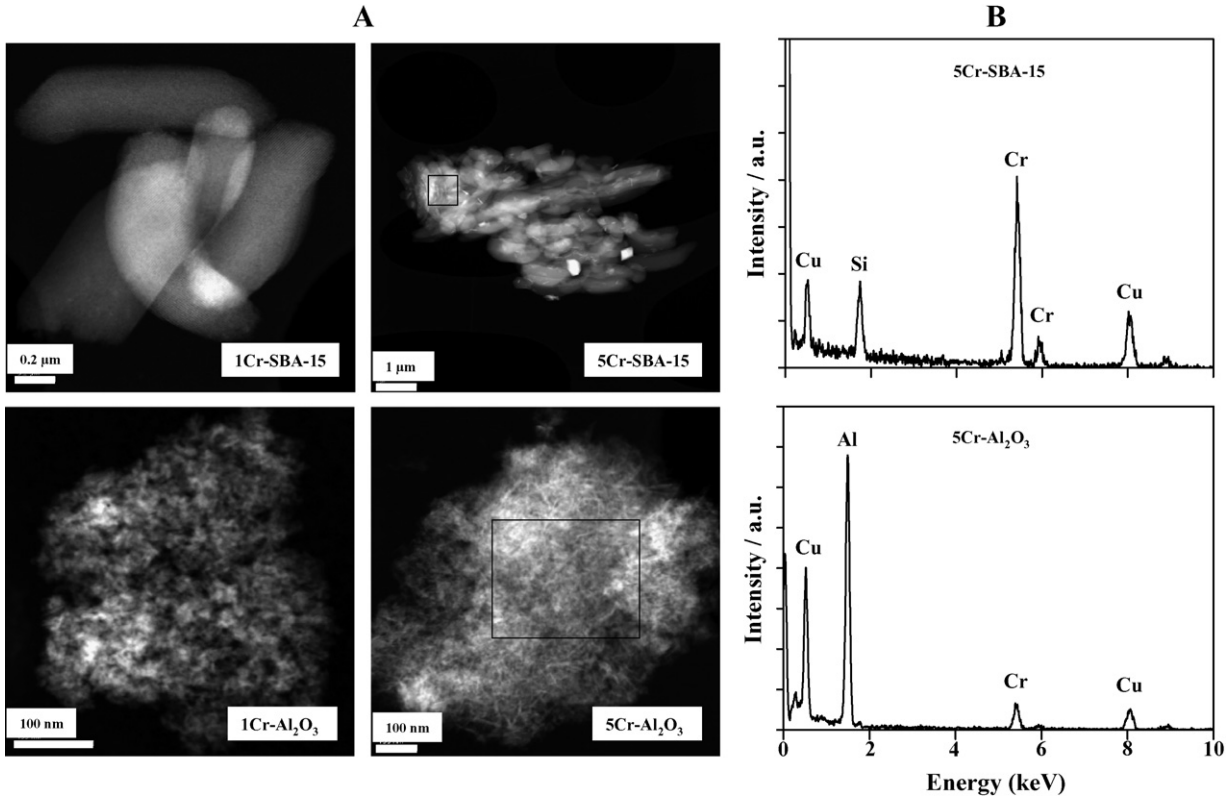

Fig. 4. Scanning transmission electron microscope (STEM) images of the catalysts (A) and energy dispersive X-ray spectroscopy (EDXS) collected in the marked area of the corresponding STEM images of the catalysts (B).

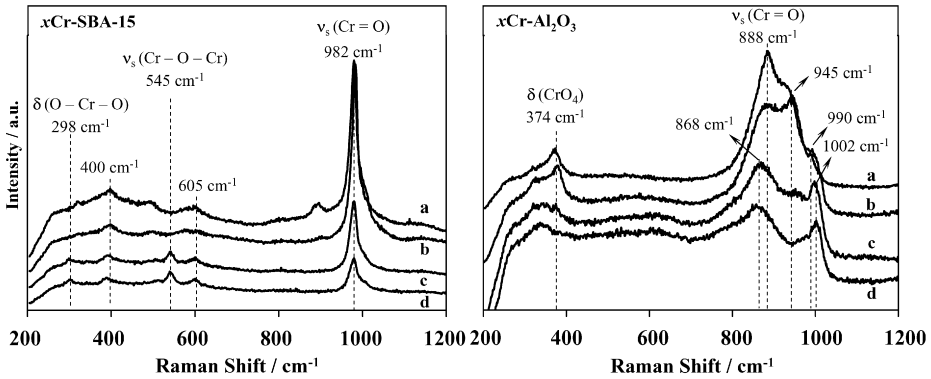

Fig. 5. UV-Raman spectra of the catalysts: a, b, c and d correspond to 0.5, 1, 5 and 10 wt% Cr catalysts, respectively.

also observed at 895 and 400 cm^{-1}. The former band is often assigned to hydrated dichromate ($Cr_2O_7^{2-}$) and the latter may be due to the bending mode of CrO_2 units [23,25,28]. These observations suggest that chromium is highly dispersed in the catalyst, especially in the form of monochromate species. With increasing Cr content from 0.5 to 10 wt%, the band at ~980 cm^{-1} decreases drastically in intensity, the band at ~895 cm^{-1} completely disappears and the band at around 400 cm^{-1} is virtually not affected, whilst new bands at 545 and 298 cm^{-1} emerge (Figs. 5c and 5d). The band at 545 cm^{-1} is typical of symmetric stretching mode of Cr–O–Cr units in Cr_2O_3 crystals, whereas the band at 298 cm^{-1} is due to bending mode of O–Cr–O units. These results suggest that crystalline Cr_2O_3 particles are formed at the expense of monochromate species by increasing Cr content, which confirms the results of XRD and STEM.

Besides the characteristic Raman bands of chromium oxo species, bands of support SBA-15 are also observed. At low Cr content (⩽1 wt% of Cr), Raman bands of the support SBA-15 appear at 495, 605 and 807 cm^{-1} (Figs. 5a and 5b) which are assigned to different siloxane rings of SBA-15 [50]. The 495 and 807 cm^{-1} bands disappear at higher Cr content (⩾5 wt%) whereas, the band at 605 cm^{-1} more or less completely vanishes at 1 wt% Cr but again reappears at ⩾5 wt% Cr, however slightly blue shifted to 603 cm^{-1}. This could be due to either the symmetric stretching of Cr–O–Cr units in polymeric Cr species [23] or the surface three membered siloxane rings of SBA-15 [50]. The former is possible because both the catalysts largely dominated by crystalline Cr_2O_3 particles that are formed at the expense of monochromate species, which were previously homogeneously covering the surface of SBA-15. However, the latter is also possible because the surface might have been re-exposed in the catalysts.

As mentioned previously, the Raman spectra of *x*Cr–Al_2O_3 is different from that of *x*Cr–SBA-15 and show broad and multiple bands between 750–1050 cm^{-1} (Fig. 5). These bands are often observed for Cr supported on Al_2O_3 [24–29]. The Raman spectrum of 0.5Cr–Al_2O_3 shows a main broad band centered at 888 cm^{-1} which contains shoulders at 935 and 990 cm^{-1} and, in addition, a band at 374 cm^{-1}. The pair of 888 and 374 cm^{-1} bands is often assigned to symmetric stretching and bending modes of hydrated surface mono chromate species (CrO_4^{2-}) [24]. Bands at 935 and 990 cm^{-1} appear as shoulders to the main band at 888 cm^{-1} and are tentatively attributed to hydrated di- and trichromates, respectively [24,29]. All the Raman bands are also present in 1Cr–Al_2O_3 however, formation of di- and trichromate species is more pronounced as evidenced by the increased intensity of the corresponding bands (~945 and ~990 cm^{-1}) at the expense of monochromate species represented by the band at 888 cm^{-1} that decreased in intensity. The intensity of the latter band further decreases and the band at 374 cm^{-1} more or less completely disappears in spectra 5Cr–Al_2O_3 and 10Cr–Al_2O_3. New Raman bands at ~868, 956 and 1002 cm^{-1} emerge along with broad shoulders (at ~770 and ~888 cm^{-1}) to the band 868 cm^{-1}. All these bands point to the formation of polymeric species at the expense of mono and dimeric species [27]. However, it should be noted that the formation of large Cr_2O_3-like clusters was not detected, unlike on SBA-15, as evidenced by the absence of a Raman band at ~550 cm^{-1} which is typical of such clusters. This suggests that the dispersion of Cr (at ⩾5 wt%) is higher on the support Al_2O_3 than that on SBA-15. Moreover, the Raman results clearly show that molecular structure of Cr species (that include chemical nature) is different on both the supports and is dependent on the nature of the support, which is indeed in line with previous reports [24]. This can be attributed to the presence of different degrees of surface hydroxyl groups on the supports which are abundant on alumina than on SBA-15. These surface hydroxyl groups play a critical role in the dispersion of Cr species by reacting with it's precursor during the preparation and pre-treatment procedures that lead to the anchoring of Cr as chromium oxo species to the support. Consequently, it prevents the formation of large chromium oxide clusters on alumina by trapping chromium oxo species within the pores as evidenced by the decreased pore size distribution in 5Cr–Al_2O_3 and 10Cr–Al_2O_3 (Fig. 2B and Table 1). This implies formation of mono and oligomeric (including dimers) Cr species on the support Al_2O_3 as evidenced by Raman spectroscopy. Differently, due to the lack of enough surface hydroxyl groups on support SBA-15, excess of Cr tends to precipitate as Cr_2O_3 crystals. In particular, at the external surface of SBA-15 where the particles can grow further in size without affecting the pore geometry of the support as evidenced by N_2-physisorption, XRD and STEM–EDXS. However, the effect of textural properties of the supports, such as interstitial voids between the support particles, on the distribution of Cr species may not be completely ruled out. Nonetheless, these observations are also in excellent agreement with previous studies which suggest that Cr tends to form large Cr_2O_3 clusters more easily when it is supported on SiO_2 than that on Al_2O_3 [24,26].

Table 2
Observed position (eV) and intensity (normalized absorbance) of pre-edge peak and edge in XANES of different model compounds and the catalysts.

Sample	Pre-edge peak		Edge	
	Position	Intensity	Position	Intensity
Na_2CrO_4	5993.38	0.725507	6006.83	0.635727
$K_2Cr_2O_7$	5993.47	0.704621	6007.01	0.632194
CrO_3	5993.65	0.683555	6005.06	0.614628
CrO_2	5993.46	0.144916	6002.74	0.595882
			6006.80[a]	0.973937[a]
Cr_2O_3	5990.69	0.0537905	6001.26	0.660262
	5993.96[a]	0.108647[a]	6005.30[a]	1.10521[a]
5Cr–SBA-15	5993.86	0.341949	6003.34	0.619583
10Cr–SBA-15	5993.57	0.23393	6002.99	0.664745
5Cr–Al_2O_3	5993.66	0.451422	6005.65	0.750558
10Cr–Al_2O_3	5993.38	0.294317	6003.57	0.66029

[a] Resolved second feature.

The structure of Cr species in the catalysts is further investigated by XAS which provides information not only on the oxidation and coordination state (XANES) of the Cr species but also on the degree of clustering (EXAFS) [36]. Therefore, XAS studies were primarily conducted to support the conclusions derived from Raman and other characterization techniques and to examine the Cr speciation in the catalysts in minute detail.

3.1.5. X-ray absorption spectroscopy (XAS)

XANES

For comparative purposes, XANES spectra of various model compounds that have well defined oxidation and coordination states of Cr species are compared in Fig. 6A. It can be readily seen that Cr in tetrahedral (T_d) coordination with an oxidation state of (VI) (CrO_3, $K_2Cr_2O_7$ and Na_2CrO_4) shows a sharp pre-edge peak. The position, intensity and shape of the peak are, however, slightly different for these model compounds (Table 2) indicating the different nature of Cr centers in these compounds. The pre-edge peak is frequently assigned to dipole forbidden electron transition from 1s → 3d (energy states: $A_1 \rightarrow E$) [15,26,35,36,51]. This transition occurs due to the lack of inversion center at the Cr metal center in T_d coordination, hence it is a Laporte allowed transition. Likewise, symmetry of Cr sites in octahedral (O_{ct}) coordination is much higher as compared in T_d thus, the electron transition from 1s → 3d is difficult due to the presence of the inversion center. Therefore, the intensity of the pre-edge peak is much lower for α-Cr_2O_3 and CrO_2 while Cr(II) in square planar in Cr acetate shows a shoulder at 5.996 keV, which is located almost on the edge. These differences in oxidation and coordination state of Cr species are also reflected in the edge position of the model com-

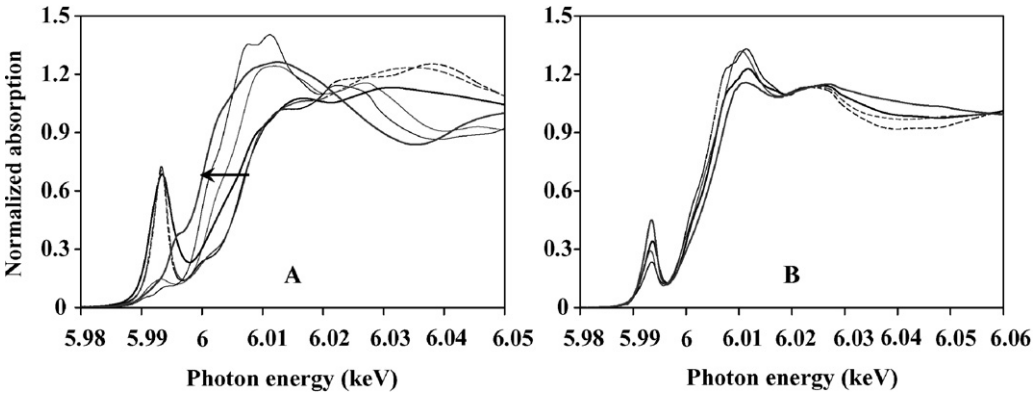

Fig. 6. Ex situ XANES of the model compounds (A): $K_2Cr_2O_7$ (dark gray thin broken line), Na_2CrO_4 (black thin broken line), CrO_3 (black thick full line), Cr acetate (dark gray thick full line), CrO_2 (dark gray thin full line) and Cr_2O_3 (black thin full line) and the catalysts (B): 5Cr–SBA-15 (black thick full line), 10Cr–SBA-15 (black thin broken line), 5Cr–Al_2O_3 (gray thick full line) and 10Cr–Al_2O_3 (gray thin broken line).

pounds. In general with increasing symmetry at Cr metal centers and with decreasing oxidation state from (VI) to (II), the edge position is red shifted (Fig. 6A).

Against this background, it can be clearly seen from Fig. 6B that the pre-edge peak position and intensity as well as the edge positions are quite different for the catalysts (Table 2). It should be noted that to obtain a satisfactory signal to noise ratio of XAS spectra in the transmission mode a reasonable Cr content (e.g., 4 wt%) is required [26,36] hence, only the catalysts with $\geqslant$5 wt% Cr are shown. The intensity of the pre-edge peak is, in general, higher for *x*Cr–Al_2O_3 than that for *x*Cr–SBA-15. It decreases with increasing Cr content from 5 to 10 wt% which is more pronounced for the latter catalysts (Table 2). Also, it can be seen from Fig. 6B and Table 2 that the pre-edge peak of *x*Cr–Al_2O_3 is centered at a slightly lower energy (though it should be treated with caution) than that of *x*Cr–SBA-15, suggesting the energy required for an electron transition from 1s $\rightarrow$ 3d is lower for Cr species supported on the former catalysts. This is due to the fact that interactions between support and Cr species are greater in *x*Cr–Al_2O_3 than in *x*Cr–SBA-15 due to the presence of abundant surface hydroxyl groups in the former (as discussed for Raman results, see above) [36]. This mainly has two implications on the structure and electronic properties of Cr species: (i) the interactions between support and Cr species govern the symmetry of the Cr centers and (ii) the distance between the energy states is influenced by the ligand effect. Accordingly, the edge position of *x*Cr–Al_2O_3 is more close to CrO_3, $K_2Cr_2O_7$ and Na_2CrO_4 while that of *x*Cr–SBA-15 coincides with that of α-Cr_2O_3 and CrO_2 (Table 2). This suggests that in *x*Cr–Al_2O_3, Cr species are mainly present as Cr(VI) in T_d coordination while in *x*Cr–SBA-15, Cr(III) sites in O_{ct} coordination are the dominating species. Semi-quantitative data (not shown) on the composition of different kinds of Cr species present in the catalysts, obtained by simulating the experimental XANES spectra of the catalysts with the available model compounds, also point to the same. These results confirm that the nature of Cr species is different in the catalysts and is dependent on the nature of the support and Cr content, in accordance with Raman results (Fig. 5).

EXAFS

The structure of Cr species in the catalysts is further studied by the k^2-weighted Fourier transform (FT) of EXAFS functions, non-phase shift corrected. The EXAFS spectra of 5Cr–SBA-15 and 5Cr–Al_2O_3 are compared with appropriate model compounds (based on the quantitative data obtained by simulation of experimental XANES spectra) for the sake of clarity (Fig. 7). Starting with the model compounds, α-Cr_2O_3 shows three main peaks at 1.57, 2.62 and 3.57 Å which were frequently observed for the same compound and were assigned to first, second and third shell contributions, respectively, of Cr(III) in an O_{ct} coordination [15,36,52]. The model compound Na_2CrO_4 in which Cr(VI) is in T_d coordination exhibits three main peaks at 1.46, 2.07 and 2.87 Å that are arising from first, second and third shell contributions, respectively. CrO_3 that also contains Cr(VI) in T_d geometry exhibits only a single peak centered at 1.35 Å attributable to first shell contribution and no significant contributions from the higher shells, are observed. From the spectra of these model compounds it can be readily seen that the position and the intensity of the peaks are quite different (Fig. 7). The different peak position is due to different Cr–O bond distances in O_{ct} and T_d coordinations which are shorter in the latter state. The intensity of first shell peak is much weaker for CrO_3 than that of Na_2CrO_4 and α-Cr_2O_3, indicating a greater disorder in Cr T_d units. This could also explain the absence of contributions from the higher shells in the spectrum of CrO_3.

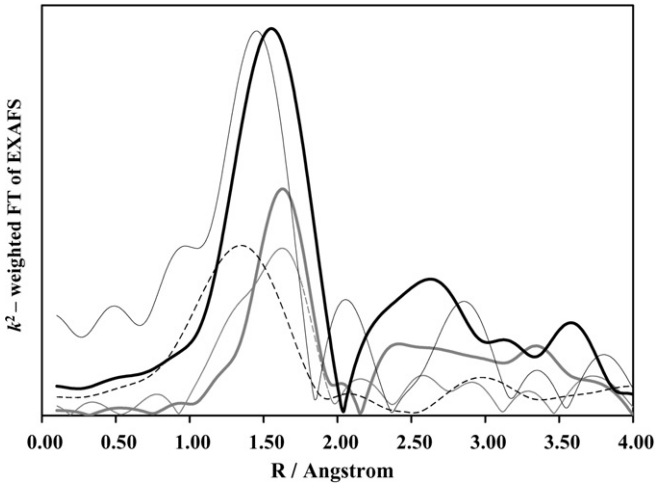

Fig. 7. Ex situ EXAFS (k^2-weighted, phase uncorrected and Fourier transform) of the model compounds and the catalysts: Cr_2O_3 (black thick full line), Na_2CrO_4 (black thin full line), CrO_3 (black thin broken line), and 5Cr–SBA-15 (gray thick full line) and 5Cr–Al_2O_3 (gray thin broken line).

Based on this, 5 and 10 wt% Cr catalysts are analyzed by EXAFS (k^2-weighted FT and non-phase shift corrected). For the sake of clarity, only 5Cr–SBA-15 and 5Cr–Al_2O_3 are shown in Fig. 7. For 5Cr–SBA-15, three main peaks are observed at 1.64, 2.41 and 3.36 Å. The peak at 1.64 Å indicates the single Cr–O bond nature and is longer than that in model α-Cr_2O_3. Taking account of Raman results, the peak can be attributed to either isolated Cr(VI) or Cr(III) in clusters [36]. The second and third shell peaks are similar to that observed for α-Cr_2O_3 indicating the existence of crystalline α-Cr_2O_3 particles in the catalyst. Similar peaks are ob-

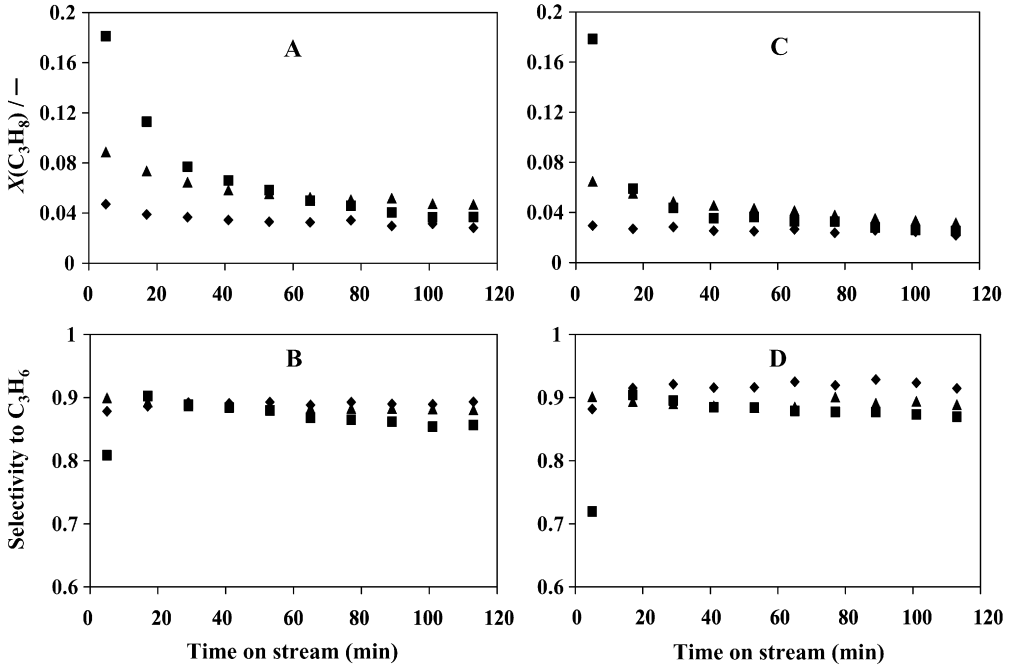

Fig. 8. Dehydrogenation of propane over 0.5Cr–SBA-15 (◆), 1Cr–SBA-15 (▲) and 5Cr–SBA-15 (■): C_3H_8 conversion and selectivity to C_3H_6 over fresh catalysts (A, B) and after first regeneration (C, D), respectively. Conditions as described in Section 2.

served for 10Cr–SBA-15 at 1.66, 2.62 and 3.50 Å which are more intense and well defined, in particular the latter two peaks, than that in 5Cr–SBA-15. The peaks at 2.62 and 3.50 Å coincide well with that of model α-Cr_2O_3 indicating the presence of well ordered chromium oxide crystals in the catalysts, in line with XRD, STEM, Raman and XANES. Differently, 5Cr–Al_2O_3 and 10Cr–Al_2O_3 show a peak centered at 1.64 Å which contains a pronounced shoulder at 1.34 Å and the contributions from higher coordination shells are only weak confirming no significant cluster formation in the catalysts. The shoulder at 1.34 Å coincides with that of a main peak of CrO_3 model compound indicating a short Cr–O bond distance like in T_d coordination. As evidenced by Raman, these catalysts contain oligomeric species which are, however, not detected by EXAFS suggesting that these species are very small in size with greater disorder. These results are in excellent agreement with the other characterization results discussed above.

In summary, N_2-physisorption data of the Cr catalysts show that the structure of the support is virtually intact even after Cr loading onto the support followed by subsequent pre-treatments (drying and calcination). The Cr speciation is dependent on the nature of the supports and Cr loading as evidenced by XRD, STEM–EDXS, UV-Raman, XANES and EXAFS. At $\leqslant$1 wt% Cr loading, in general, Cr species are well dispersed on both the supports SBA-15 and Al_2O_3. In particular, on SBA-15 they are merely isolated Cr(VI) in T_d coordination while on Al_2O_3, oligomers (including dimers) are also formed as evidenced by the Raman bands. Considering the Raman and XANES results, it can be suggested that the nature of Cr species on these supports is different. At $\geqslant$5 wt% Cr loading, the dispersion of chromium decreases implying the formation of α-Cr_2O_3 crystals at the expense of isolated sites on SBA-15 while, the dispersion is still high on Al_2O_3 and no detectable clusters have formed.

3.2. Dehydrogenation of propane

The catalytic performance of the catalysts was studied to comprehend the relationship between the structure of Cr species as evidenced by different characterization techniques and the DHP activity. It should be mentioned that the catalytic data of 10Cr–SBA-15 and 10Cr–Al_2O_3, which are similar to 5 wt% Cr catalysts with respect to the nature and distribution of Cr species as evidenced by characterization results, are not presented due to technical problems in the TEOM setup. Fig. 8 shows C_3H_8 conversion and selectivity to C_3H_6 over catalysts *x*Cr–SBA-15 at 853 K. Initially, complete combustion of C_3H_8 was observed hence, initial conversion values were taken after 5 min steady state analysis. In general, conversion of C_3H_8 increased with Cr content from 0.5 to 5 wt%. In particular, 0.5Cr–SBA-15, which contains exclusively isolated Cr species in T_d coordination as evidenced by the Raman spectrum (Fig. 5a), shows reasonable C_3H_8 conversion and it gradually decreases with time, indicating the involvement of the isolated Cr species in DHP. Similarly, by increasing the Cr content from 0.5 to 1 wt%, which also contains exclusively isolated sites in T_d coordination (Fig. 5b), the C_3H_8 conversion is almost doubled. This confirms the involvement of the isolated Cr species in the DHP reaction. However, it should be noted that C_3H_8 conversion did not increase by five fold when the Cr content is increased from 1 to 5 wt%. Moreover, the conversion dramatically decreases with time as compared with 0.5 and 1 wt% Cr catalysts (Fig. 8). This is due to the fact that at this Cr loading, crystalline Cr_2O_3 particles are formed at the expense of isolated Cr species in 5Cr–SBA-15 as evidenced by various characterization techniques. Thus, only a fraction of Cr sites are available for DHP which in turn leads to lower catalytic activity. The dramatic drop in the conversion may indicate the involvement of Cr species, a majority of which are different in nature as compared to the Cr sites in 1Cr–SBA-15. For instance, the accessible Cr sites on the surface of crystalline Cr_2O_3 particles seem more sensitive to deactivation by coke formation [11,17,18], than isolated Cr sites. This also suggests a possible ensemble effect on the activity and deactivation. The influence of the distribution of Cr species which is markedly different in the catalysts is also reflected on the selectivity to C_3H_6 (Fig. 8B). The initial selectivity to C_3H_6 is almost 80% on 5Cr–SBA-15 while it is ~90% on 0.5Cr–SBA-15 and 1Cr–SBA-15. These results evidenced that isolated Cr species are more active, selective and stable in the first DHP run than crystalline Cr_2O_3 particles.

Furthermore, to investigate the behavior of Cr species in the second DHP run after oxidative treatment at 753 K for 1 h, the

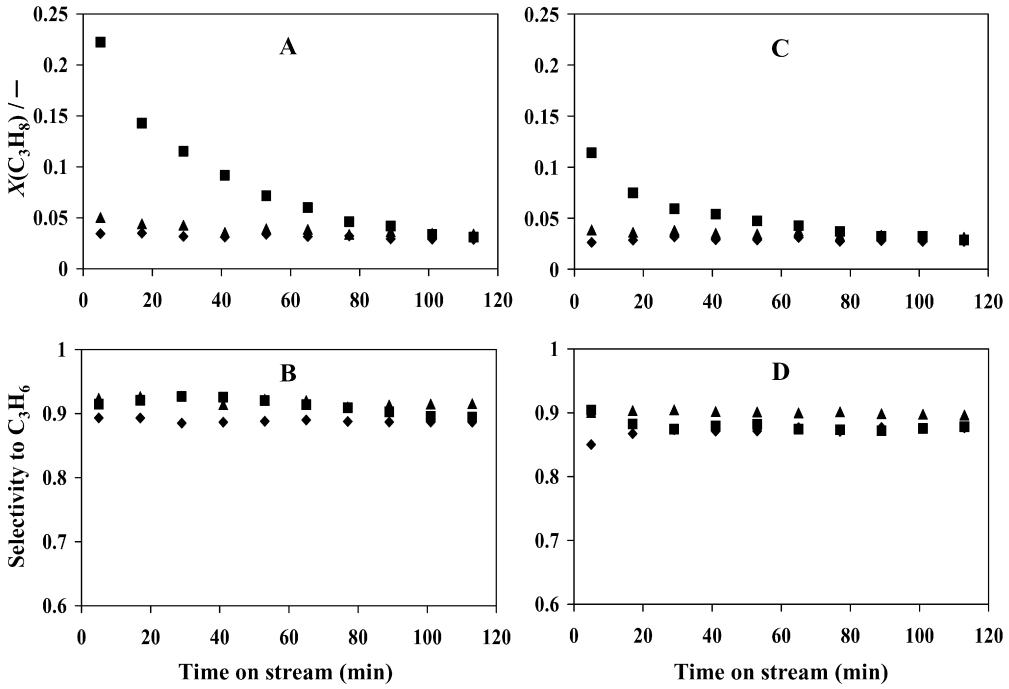

Fig. 9. Dehydrogenation of propane over 0.5Cr–Al_2O_3 (◆), 1Cr–Al_2O_3 (▲) and 5Cr–Al_2O_3 (■): C_3H_8 conversion and selectivity to C_3H_6 over fresh catalysts (A, B) and after first regeneration (C, D), respectively. Conditions as described in Section 2.

catalysts were regenerated after 120 min on stream (after the first run). Figs. 8C and 8D shows the conversion of C_3H_8 and selectivity to C_3H_6 over these catalysts after first oxidative regeneration, respectively. The initial activity of catalysts 0.5Cr–SBA-15 and 1Cr–SBA-15 was not completely recovered while that of 5Cr–SBA-15 was more or less completely recovered. On the one hand, it suggests that isolated sites may not be completely regenerated under these conditions or a fraction of isolated sites might have been irreversibly deactivated. On the other hand, it suggests that the accessible Cr sites on the surface of Cr_2O_3 crystals may almost be completely regenerated. However, the activity drastically decreased during on stream for all the catalysts, being more significant for crystals containing 5Cr–SBA-15. This could be due to the rearrangement of the molecular structure of Cr species in the catalysts during the reaction and regeneration process. Accordingly, this could also explain the modified C_3H_6 selectivities over the same catalysts (Fig. 8D) as compared to the first run (Fig. 8B).

The catalytic performance of *x*Cr–Al_2O_3 is shown in Fig. 9. Catalysts 0.5Cr–Al_2O_3 and 1Cr–Al_2O_3 contain isolated Cr species besides a fraction of oligomeric species (including dimers), which is higher in the latter as shown by Raman spectra (Figs. 5a and 5b). However, the conversion of C_3H_8 is, in general, comparable over both the catalysts. Specifically, 1Cr–Al_2O_3 shows slightly higher C_3H_8 conversion in the initial period than that on 0.5Cr–Al_2O_3. As evidenced from the conversion profiles, the decrease in the catalytic activity is nominal during the time on stream. Interestingly, the catalytic activity of 0.5Cr–Al_2O_3 and 1Cr–Al_2O_3 is lower than their counter SBA-15 catalysts and C_3H_8 conversion did virtually not increase by increasing the Cr content from 0.5 to 1 wt%, which is opposite to that observed for the latter catalysts (Fig. 8). Nonetheless, the selectivity to C_3H_6 is in general comparable over these catalysts. The observed differences in the activity of these two kinds of catalysts can be attributed to the different nature of Cr species in the catalysts as evidenced by Raman and XANES (Table 2). Accordingly, it can be suggested that Cr species in T_d coordination stabilized on SBA-15, reflected by a Raman band at 982 cm^{-1}, are more active than that of Cr species supported on Al_2O_3, reflected by a Raman band at 888 cm^{-1}.

By comparing the catalytic activity of 1Cr–Al_2O_3 and 5Cr–Al_2O_3, it is evident that the initial C_3H_8 conversion is almost five times higher on the latter which coincides well with the increased amount of Cr content. It should be mentioned that unlike 5Cr–SBA-15, 5Cr–Al_2O_3 contains both isolated and oligomeric Cr species but no Cr_2O_3-like clusters as evidenced by various characterization results. Accordingly, 5Cr–Al_2O_3 shows higher activity, selectivity (Fig. 9B) and stability (as evidenced by a gradual decrease in activity) than that of 5Cr–SBA-15, which is dominated by crystalline Cr_2O_3 particles. Again it suggests that the function (activity, selectivity and stability) of Cr species is different in the catalysts, which seems to depend on the nature of the support that has been used for stabilizing them.

The catalytic performance of the regenerated (after the first run) catalysts in a second DHP run was also studied for *x*Cr–Al_2O_3. It can be seen from Figs. 9C and 9D that the initial activity of the catalysts was not recovered. This is similar to the behavior observed for 0.5Cr–SBA-15 and 1Cr–SBA-15 which exclusively contain isolated Cr species. The loss of initial activity is severe for 5Cr–Al_2O_3 than for catalysts with $\leqslant 1$ wt% Cr. By comparison of the catalytic performances of the regenerated *x*Cr–Al_2O_3 and *x*Cr–SBA-15, it can be suggested that oligomeric Cr species are more sensitive to reaction and regeneration processes under which they may undergo structural changes, as discussed for 5Cr–SBA-15 though, to different extents. Considering the size of chromium oxide clusters, it is reasonable to speculate that such a change could significantly influence the nature of Cr species in smaller oligomers than that in crystalline Cr_2O_3. Accordingly, the catalytic activity of Cr species is influenced to different degrees in 5Cr–Al_2O_3 and 5Cr–SBA-15. Nonetheless, the loss of initial activity of the catalysts in the second DHP run could also be due to the deactivation of Cr species by coke that maybe difficult to remove under these regeneration conditions. The loss of activity during on stream is faster over the regenerated 5Cr–Al_2O_3 than that on fresh catalyst while, it is nominal over fresh and regenerated *x*Cr–Al_2O_3 catalysts with $\leqslant 1$ wt% Cr. However when the stability of the regenerated 5Cr–Al_2O_3 and 5Cr–SBA-15 is compared, it is evident that the former shows better stability and is similar to the behavior observed for the fresh

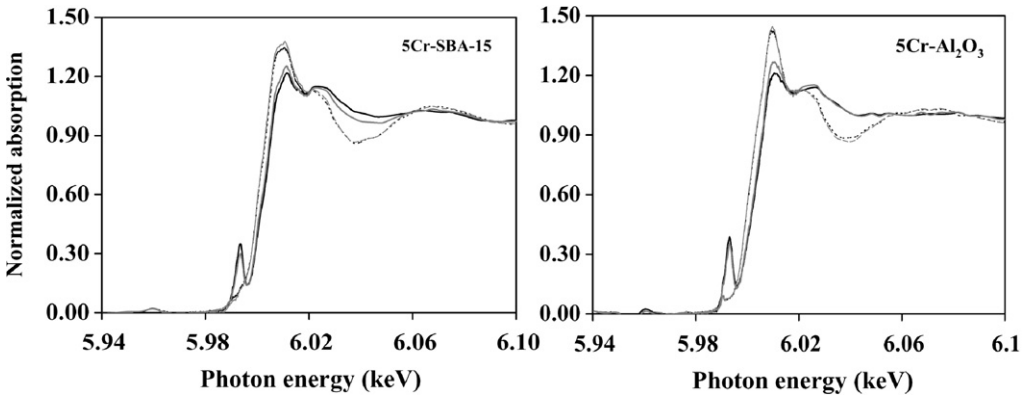

Fig. 10. In situ XANES of the catalysts taken at 823 K: after oxidative pre-treatment (black full line), after 90 s (black broken line) and 15 min DHP (gray broken line) and after regeneration (gray full line). Reaction conditions as described in Section 2.

catalysts. Selectivity to C_3H_6 is slightly lower over the regenerated catalysts than on the fresh catalysts.

Based on the characterization results and catalytic performance of *x*Cr–SBA-15 and *x*Cr–Al_2O_3, it can be concluded that the catalytic activity of Cr species strongly depends on the nature of the support on which they have been stabilized. Accordingly, Cr species stabilized on SBA-15 as isolated sites in T_d coordination are remarkably more active than their counter parts supported on Al_2O_3 and on the surface of crystalline Cr_2O_3 particles present on SBA-15. Differently, oligomeric Cr species anchored on Al_2O_3 are more active than isolated Cr species present on the same support. However, such a comparison of Cr species (isolated vs oligomers) supported on SBA-15 is not possible in this study due to the lack of Cr–SBA-15 that contains mainly oligomers like in 5Cr–Al_2O_3.

3.3. In situ X-ray absorption spectroscopy (XAS)

The objective of in situ XAS (XANES and EXAFS) studies is to understand the behavior of Cr species during the DHP on fresh and regenerated catalysts based on the changes that occur in oxidation and coordination states of Cr species. To this end, 5 wt% Cr catalysts were selected from the series of *x*Cr–SBA-15 and *x*Cr–Al_2O_3 and subjected to pre-treatment, reaction (first DHP run), regeneration and reaction (second DHP run) at 823 K. The temperature is comparable to that of steady-state catalysis experiments (853 K) at which the catalysts have shown substantial DHP activity.

3.3.1. 5Cr–SBA-15

The pre-edge peak in XANES spectra of 5Cr–SBA-15 corresponding to Cr(VI) in T_d coordination disappeared, edge (white line) position shifted towards lower energy and increased in intensity after DHP for 90 s, as seen by comparison of the spectra of the catalyst after oxidative pre-treatment (hereafter mentioned as initial spectrum) and after DHP for 90 s (Fig. 10). The XANES spectrum does virtually not change even after 15 min DHP as compared to the spectrum taken after 90 s (see Fig. 10). From these observations, it can be concluded that Cr(VI) in T_d coordination is reduced within 90 s and the average Cr coordination number is increased (>4, though a definitive conclusion on the number cannot be made) upon contact with C_3H_8. Similar changes in XANES spectra of Cr-catalysts were observed upon introduction of either C_3H_8 or C_2H_4 on to the oxidized catalysts [16,36]. However, the changes in the XANES spectra of the catalyst are not completely reversible upon re-oxidation in a flow of O_2/He at the same temperature (823 K) for 1 h. The intensity of the pre-edge peak is considerably lower and the white line is slightly higher than in the initial spectrum. This is an indication of the loss of a fraction of isolated Cr(VI) sites in T_d coordination in favor of Cr(III) in O_{ct} state, perhaps clustered ones, suggesting that structural changes have occurred in Cr species upon reaction and regeneration. This could explain the altered catalytic properties of regenerated 5Cr–SBA-15 as seen in the second DHP run as compared to the fresh catalyst in the first run (Fig. 8). Finally, switching back to C_3H_8/He flow for 1 h (the second run) lead to an identical XANES spectrum (not shown for the sake of clarity) that was observed after 15 min DHP in the first run indicating that similar changes have occurred even after 1 h DHP.

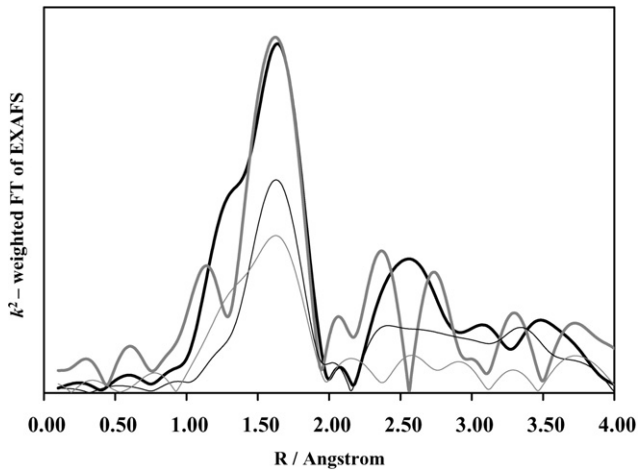

Fig. 11. EXAFS (k^2-weighted, phase uncorrected and Fourier transform) of 5Cr–SBA-15 (black) and 5Cr–Al_2O_3 (gray): before DHP (thin line) and after 1 h DHP in second run (thick line). Reaction conditions as described in Section 2.

The EXAFS spectra (k^2-weighted FT and non-phase shift corrected) of 5Cr–SBA-15 before and after 1 h DHP in the second run are shown in Fig. 11. By comparison of the spectra, it is evident that major changes have occurred after the reaction. The intensity of the main peak located at 1.64 Å is significantly increased and a shoulder emerged at 1.34 Å. Also, the peaks in the second and third coordination shells grew in intensity as compared to the peaks observed in the spectrum of the fresh catalyst (before the reaction) (Fig. 11). Considering the XANES results, isolated Cr(VI) species in T_d coordination are reduced which in turn lead to a lower oxidation state (mostly, III) and hence, increased Cr–O bond distances can be expected due to the large ionic radius of the reduced Cr atoms than that of Cr(VI). Therefore, in the EXAFS spectrum the shoulder at 1.34 Å is not expected which indicates short Cr–X (X = O or C) bond nature (perhaps, double bond like in T_d coordination). In fact such a peak attributable to Cr–O bond decreased after reduction of Cr–Al_2O_3 by H_2 as reported in [14]. Similarly, the dramatic increase in intensity of the main peak at 1.64 Å is due to the increase in average coordination number in Cr coordination sphere. This could be either by ligation of C atoms

of coke with Cr species [36] or by severe aggregation [16]. As evidenced by other characterization techniques, the catalyst is already dominated by crystalline α-Cr_2O_3 particles, hence it is unlikely that the formation of additional clusters or structural rearrangement of Cr species could increase the intensity of the peak to such an extent. For instance, a study [14] reported the structural rearrangement of surface Cr species into more crystalline aggregates upon reduction of a typical industrial like Cr–Al_2O_3 (13 wt% Cr) with H_2 in which the intensity of the peaks arising from first and second shell contributions is virtually the same. Conversely, it is well known that carbon deposits can readily form during DHP [11, 17,18], which could lead to the formation of Cr–C bonds on a coked catalyst. It should be noted that the EXAFS spectrum was recorded at room temperature in He flow after 1 h DHP at 823 K. Thus, the increase in the coordination number of the reduced Cr species is likely due to coke, as also evidenced by the increased white line in in situ XANES spectra taken during DHP. Furthermore, a recent study on Philips catalyst by XAS showed that upon introduction of C_2H_4 on to an oxidized catalyst lead to a huge increase in the intensity of white line (in XANES) and of the peaks corresponding to first and second coordination shells (in EXAFS) [36]. These observations were attributed to coke rather than aggregation or rearrangement of surface Cr species. It is noteworthy that EXAFS cannot distinguish between Cr–O and Cr–C bonds in the first coordination shell [36]. Therefore, the observed spectral changes in our study are mostly due to the formation of coke however, a contribution from structural rearrangement of surface Cr species into more crystalline particles during DHP cannot be ruled out.

3.3.2. 5Cr–Al_2O_3

As shown in Fig. 10, the changes in XANES spectra of 5Cr–Al_2O_3 are similar to those observed for 5Cr–SBA-15 after the first and second DHP runs. In both the runs, pre-edge peak vanished and position of the edge shifted towards lower energy and the intensity of the white line is considerably higher than in the initial spectrum. Interestingly, the intensity of the white line is slightly higher than that observed for 5Cr–SBA-15. Regeneration between the two DHP runs did not completely restore the initial XANES spectrum. However, significantly the isolated Cr species are more or less completely restored as evidenced by the pre-edge peak, which is quite different from 5Cr–SBA-15 in which a fraction of isolated Cr species were lost in favor of clusters. Furthermore, the intensity of the white line is significantly higher in the regenerated spectrum than in the initial and in the regenerated spectrum of 5Cr–SBA-15. This indicates a significant increase in the coordination number of Cr species while retaining almost all isolated Cr sites in the catalysts after regeneration which in turn suggests that oligomeric Cr species are more sensitive to reaction and regeneration processes than the isolated Cr sites and Cr sites on the surface of Cr_2O_3 crystals in 5Cr–SBA-15. Therefore, it can be proposed that oligomers have aggregated, to some extent, into larger clusters during the reaction and regeneration implying altered nature and distribution of Cr species in the catalyst. This is in excellent agreement with the catalytic data that show dramatic drop in the initial DHP activity (in the second DHP run) of the catalyst after regeneration (Fig. 9). These results confirm that small oligomeric Cr species supported on γ-Al_2O_3 are more active than isolated Cr sites and large oxide clusters.

The corresponding k^2-weighted FT-EXAFS spectra (non-phase shift corrected) of 5Cr–Al_2O_3 before and after 1 h DHP in the second run are compared in Fig. 11. Significant changes can be seen in the spectrum after the reaction. The intensity of the main peak centered at 1.64 Å increased significantly, which is slightly higher in intensity than that observed for 5Cr–SBA-15, and the shoulder at 1.34 Å disappeared. Additionally new peaks, with respect to the main peak, appeared at shorter (1.16 Å) and larger distances (2.07, 2.38, 2.75, 3.31 and 3.72 Å), which were not observed in the initial spectrum. As evidenced by other characterization results, the fresh 5Cr–Al_2O_3 catalyst contains highly dispersed Cr species and no detectable Cr oxide clusters. Furthermore, it should be noted that support γ-Al_2O_3 is more acidic than SBA-15 [38] which, is highly favorable for coke formation [11,17,18]. Based on this, the peak at 1.16 Å (indicating the short double bond nature), the dramatic increase in the intensity of the main peak at 1.64 Å and significant contributions from higher coordination shells (>2 Å) are highly likely due to the linking of C atoms (in coke) with Cr species that increases the average coordination number of Cr sites. However, formation of chromium oxide clusters during DHP cannot be ruled out, as claimed in [16]. Any attempt to derive quantitative data under such a scenario could lead to a biased spectral analysis hence, quantitative data derived from these EXAFS spectra are neither presented nor discussed.

4. Relationship between the structure and catalytic function of Cr species

Characterization of *x*Cr–SBA-15 and *x*Cr–Al_2O_3 by various techniques revealed that the nature and distribution of Cr species (monomers, oligomers and crystalline Cr_2O_3 particles) is a function of the support. It also depends on the Cr loading on a given support. At low Cr content ($\leqslant$1 wt% Cr), exclusively isolated Cr species in T_d coordination are formed on SBA-15 while oligomeric species besides isolated sites are formed on Al_2O_3. However, the nature of Cr species on both the supports is different as evidenced by Raman and XANES. At high Cr content ($\geqslant$5 wt% Cr), these isolated Cr species decreased in favor of clusters and the size of which is determined by the kind of support employed. Crystalline Cr_2O_3 particles are exclusively formed at the external surface of SBA-15. In contrast, oligomeric species, with different degrees of oligomerization, are formed within the pore of Al_2O_3 and no Cr_2O_3 like particles are formed as concluded from XRD, STEM, Raman and XAS.

In situ XANES studies show that Cr is in highly oxidized state after oxidative pre-treatment in 5Cr–SBA-15 and 5Cr–Al_2O_3. Under DHP conditions, isolated Cr(VI) species in T_d coordination are reduced to (III) and the coordination number increases (>4) within 90 s DHP, as evidenced by the disappearance of pre-edge peak, the red shift in the edge position and increased intensity of the white line. However, from this it cannot be explicitly stated whether isolated Cr sites remain isolated or agglomerate due to the contribution of C atoms (coke) to Cr coordination. Nonetheless, most of the Cr is present as Cr(III) species under DHP conditions, in good agreement with previous reports on DHP and on similar reactions [11,13,15,16,22]. In agreement with in situ XAS studies, total combustion of C_3H_8 during the initial period of DHP was observed over all these catalysts (*x*Cr–SBA-15 and *x*Cr–Al_2O_3) before reaching a steady-state. This indicates that the high oxidation state or the initial state of Cr is responsible for this detrimental reaction but when Cr is reduced or partly deactivated by coke with time it selectively catalyzes DHP.

As far as isolated Cr species are concerned, it is reasonable to say that active DHP sites are generated during the reaction, the origin of which are Cr(VI) species in T_d coordination reflected by the pre-edge peak in XANES. This is shown schematically, as a representation of the generation of active DHP site, in Fig. 12. However, it is noteworthy that the intrinsic activity of isolated Cr species supported on SBA-15 and Al_2O_3 is markedly different as evidenced by the catalytic activity of 1Cr–SBA-15 and 1Cr–Al_2O_3 (Figs. 8 and 9). The turnover frequencies (TOFs), which were calculated for the amount of initial propylene production according to the method reported in [22], for 1Cr–SBA-15 and 1Cr–Al_2O_3 were determined to be 0.03 and 0.01 (s^{-1}), respectively. This indi-

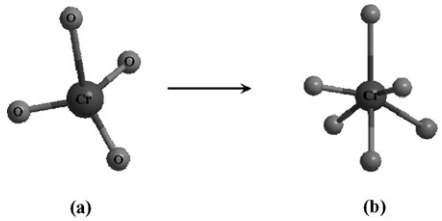

Fig. 12. Schematic mechanism of the structure of active Cr site generation during DHP at 853 K: (a) isolated Cr(VI)O_4 in T_d coordination (anchored to the support) after oxidative pre-treatments (see Section 2) and (b) generation of active DHP site after interaction with C_3H_8–Cr(III)O_xC_y. It should be noted that the number and nature of coordinating ligands in active DHP site is not conclusive from XAS (see Section 4) hence it should be treated as a virtual site.

cates that isolated Cr species anchored on the support SBA-15 are more active than those supported on Al_2O_3. The observed TOFs are smaller than those reported (0.1 mol s^{-1} mol Cr-atom^{-1}) for ethylene formation on Cr/H-ZSM-5 in ODHE [22] confirming that the nature of support determines the degree of Cr site activity. However, it should be noted that the amount of Cr in the zeolites was higher and conditions employed for the catalytic tests were different. From catalytic data of *x*Cr–SBA-15, it also appeared that besides isolated Cr sites, accessible Cr sites on the surface of crystalline Cr_2O_3 particles also participate in DHP but to a different extent.

By comparing the characterization results and catalytic data of *x*Cr–Al_2O_3, it is evident that oligomeric Cr species are much more active than isolated Cr sites. The generation of selectively active DHP oligomeric Cr sites may also proceed in a similar way as schematically shown for isolated sites in Fig. 12. However, oligomeric Cr species are more sensitive to regeneration process than isolated Cr and Cr sites on the surface of Cr_2O_3 crystals as evidenced by in situ XANES and also as reflected by the catalytic performance of *x*Cr–SBA-15 and *x*Cr–Al_2O_3 in the second DHP run (Figs. 8 and 9). This is in line with previous studies on supported Cr catalysts that conclude that oligomeric Cr is easily reducible than isolated Cr due to different degrees of interactions between the support and Cr species [14,54]. Therefore, it can be suggested that oligomeric species observed on *x*Cr–Al_2O_3 undergo structural rearrangement during the reaction and regeneration processes which could ultimately alter the nature and distribution of Cr species and hence the catalytic performance (Fig. 9). Accordingly, this explains the altered catalytic performance of regenerated *x*Cr–SBA-15 and *x*Cr–Al_2O_3 in the second DHP run. From this it also appears that the rearrangement of Cr species in oligomers compared to that in crystals has a greater influence on the catalytic property. The results clearly demonstrate that the nature and thus the degree of catalytic activity of active Cr sites in DHP certainly depend on the nature of the catalyst support. This could be one of the reasons for the controversy on the nature of active Cr sites, often compared between different Cr catalysts, in dehydrogenation of alkanes [11,12,15,16,34,53]. The finding has a significant implication on the catalytic performance and hence on the development of DHP catalysts. Therefore, the study could be used as a guide to tune active site structure and hence to design rational catalysts for DHP as well as for similar dehydrogenation of lower alkanes.

5. Conclusions

To gain a better understanding of the structure and catalytic function of Cr species, a series of *x*Cr–SBA-15 and *x*Cr–Al_2O_3 catalysts with different nature and distribution of Cr species were prepared by incipient wetness impregnation, analyzed by various characterization techniques ex situ (N_2-physisorption, XRD, UV-Raman spectroscopy, STEM–EDXS, XANES and EXAFS) and in situ (XANES and EXAFS) and tested in DHP. Based on the results, the following main conclusions can be drawn:

- At $\leqslant$1 wt% Cr, SBA-15 contains merely isolated Cr(VI) species in T_d coordination whereas γ-Al_2O_3 contains, besides isolated sites, a fraction of oligomers (including dimers).
- At $\geqslant$5 wt% Cr, besides a fraction of monomers, crystalline α-Cr_2O_3 particles are mainly formed on SBA-15 while, remarkably such crystals are not formed rather oligomers with different degrees of nuclearity are mainly formed on γ-Al_2O_3.
- In situ XANES studies evidence that isolated Cr(VI) species in T_d coordination are immediately reduced to Cr(III) and their coordination number increased (>4) upon interaction with C_3H_8, the latter is also evidenced by in situ EXAFS.
- The intrinsic catalytic activity of Cr species (isolated or oligomers) depends on the support (SBA-15 or Al_2O_3) where they have been stabilized as evidenced by the catalytic results.
- In *x*Cr–SBA-15, isolated Cr(III) species with coordination number greater than four are more active, selective and stable than Cr sites on the surface of crystalline Cr_2O_3. In contrast, oligomeric Cr species are more active and selective than isolated Cr species stabilized on *x*Cr–Al_2O_3 for DHP. However, the former species are less stable against regeneration than the latter as evidenced from the second DHP run and in situ XANES.

Acknowledgments

The Norwegian Research Council (NFR) is gratefully acknowledged for financial support through the KOSK program. The authors thank the project team at the Swiss–Norwegian Beam Lines (SNBL) at the ESRF, France for their help during the XAS experiments.

References

[1] M. Santhosh Kumar, De Chen, J.C. Walmsley, A. Holmen, Catal. Commun. 9 (2008) 747.
[2] A.H. Tullo, Chem. Eng. News 81 (2003) 15.
[3] D. Akporiaye, S.F. Jensen, U. Olsbye, F. Rohr, E. Rytter, M. Ronnekleiv, A.I. Spjelkavik, Ind. Eng. Chem. Res. 40 (2001) 4741.
[4] P. Eisele, R. Killpack, Ullman's Encyclopedia of Industrial Chemistry, sixth ed., Willey–VCH, Weinheim, 1998.
[5] C. Demay, Petr. Technol. 429 (2000) 75.
[6] D. Sanfilippo, Catal. Technol. 41 (2000) 56.
[7] Anon, Euro. Chem. News 67 (1997) 28.
[8] M.M. Bhasin, J.H. Mccain, B.V. Vora, T. Imai, P.R. Pujado, Appl. Catal. A 221 (2001) 397.
[9] B.M. Weckhuysen, R.A. Schoonheydt, Catal. Today 51 (1999) 223.
[10] B.M. Weckhuysen, A.V. Verberckmoes, J. Debaere, K. Ooms, I. Langhans, R.A. Schoonheydt, J. Mol. Catal. A 151 (2000) 115.
[11] A. Brueckner, Chem. Commun. (2001) 2122.
[12] R.L. Puurunen, B.M. Weckhuysen, J. Catal. 210 (2002) 418.
[13] B.M. Weckhuysen, Phys. Chem. Chem. Phys. 5 (2003) 4351.
[14] S.M.K. Airaksinen, A.O.I. Krause, J. Sainio, J. Lahtinen, K.J. Chao, M.O. Guerrero-Perez, M.A. Banares, Phys. Chem. Chem. Phys. 5 (2003) 4371.
[15] Y. Wang, Y. Ohishi, T. Shishido, Q. Zhang, W. Yang, Q. Guo, H. Wan, K. Takehira, J. Catal. 220 (2003) 347.
[16] K. Takehira, Y. Ohishi, T. Shishido, T. Kawabata, K. Takaki, Q. Zhang, Y. Wang, J. Catal. 224 (2004) 404.
[17] S.J. Tinnemans, M.H.F. Kox, T.A. Nijhuis, T. Visser, B.M. Weckhuysen, Phys. Chem. Chem. Phys. 7 (2005) 211.
[18] S.M.K. Airaksinen, M.A. Banares, A.O.I. Krause, J. Catal. 230 (2005) 507.
[19] F. Cavani, N. Ballarini, A. Cericola, Catal. Today 127 (2007) 113.
[20] X. Zhang, Y. Yue, Z. Gao, Catal. Lett. 83 (2002) 19.
[21] I. Takahara, W.C. Chang, N. Mimura, M. Saito, Catal. Today 45 (1998) 55.
[22] N. Mimura, M. Okamoto, H. Yamashita, S.T. Oyama, K. Murata, J. Phys. Chem. B 110 (2006) 21764.
[23] M.A. Vuurman, I.E. Wachs, D.J. Stufkens, A. Oskam, J. Mol. Catal. 80 (1993) 209.
[24] F.D. Hardcastle, I.E. Wachs, J. Mol. Catal. 46 (1988) 173.
[25] M.A. Vuurman, I.E. Wachs, J. Phys. Chem. 96 (1992) 5008.
[26] B.M. Weckhuysen, R.A. Schoonheydt, J.M. Jehng, I.E. Wachs, S.J. Cho, R. Ryoo, S. Kijlstra, E. Poels, J. Chem. Soc. Faraday Trans. 91 (1995) 3245.

[27] B.M. Weckhuysen, I.E. Wachs, R.A. Schoonheydt, Chem. Rev. 96 (1996) 3327.
[28] T.J. Dines, S. Inglis, Phys. Chem. Chem. Phys. 5 (2003) 1320.
[29] S.D. Yim, I.S. Nam, J. Catal. 221 (2004) 601.
[30] E. Groppo, C. Lamberti, S. Bordiga, G. Spoto, A. Zecchina, Chem. Rev. 105 (2005) 115.
[31] S. De Rossi, G. Ferraris, S. Fremiotti, A. Cimino, V. Indovina, Appl. Catal. A 81 (1992) 113.
[32] F. Cavani, M. Koutyrev, F. Trifiro, A. Bartolini, D. Ghisletti, R. Iezzi, A. Santucci, G. del Piero, J. Catal. 158 (1996) 236.
[33] A. Kytokivi, J.P. Jacobs, A. Hakuli, J. Merilainen, H.H. Brongersma, J. Catal. 162 (1996) 190.
[34] A. Hakuli, A. Kytokivi, A.O.I. Krause, Appl. Catal. A 190 (2000) 219.
[35] C. Pak, G.L. Haller, Microporous Mesoporous Mater. 48 (2001) 165.
[36] E. Groppa, C. Prestipino, F. Cesano, F. Bonino, S. Bordiga, C. Lamberti, P.C. Thuene, J.W. Niemantsverdriet, A. Zecchina, J. Catal. 230 (2005) 98.
[37] D. Zhao, J. Feng, Q. Huo, N. Melosh, G.H. Fredrickson, B.F. Chmelka, G.D. Stucky, Science 279 (1998) 548.
[38] M. Santhosh Kumar, J. Perez-Ramirez, M.N. Debbagh, B. Smarsly, U. Bentrup, A. Bruckner, Appl. Catal. B 62 (2006) 244.
[39] M. Santhosh Kumar, De Chen, A. Holmen, J.C. Walmsley, Catal. Today, in press.
[40] E.P. Barrett, L.G. Joyner, P.P. Halender, J. Am. Chem. Soc. 73 (1951) 373.
[41] T. Ressler, J. Synch. Rad. 5 (1998) 118.
[42] S.J. Gurman, N. Binsted, I. Ross, J. Phys. C Solid State Phys. 17 (1984) 143.
[43] J. Perez-Ramirez, A.G. Llamas, C. Daniel, C. Mirodatos, Chem. Eng. Sci. 59 (2004) 5535.
[44] P.I. Ravikovitch, A.V. Neimark, J. Phys. Chem. B 105 (2001) 6817.
[45] H.S. Potadr, Ki-Won Jun, J.W. Bae, S.M. Kim, Y. Lee, Appl. Catal. A 321 (2007) 109.
[46] S. He, C. Sun, H. Du, X. Dai, B. Wang, Chem. Eng. J. 141 (2008) 284.
[47] L. Liu, H. Li, Y. Zhang, Catal. Today 115 (2006) 235.
[48] A.B. Gaspar, C.A.C. Perez, L.C. Dieguez, Appl. Surf. Sci. 252 (2005) 939.
[49] M. Cherian, M.S. Rao, A.M. Hirt, I.E. Wachs, G. Deo, J. Catal. 211 (2002) 482.
[50] Y. Borodko, J.W. Ager III, G.E. Marti, H. Song, K. Niesz, G.A. Somorjai, J. Phys. Chem. B 109 (2005) 17386.
[51] S. Bordiga, F. Bosherini, S. Coluccia, F. Genoni, C. Lamberti, G. Leofanti, L. Marchese, G. Petrini, G. Vlaic, A. Zecchina, Catal. Lett. 26 (1994) 195.
[52] Y. Ma, S.L. suib, T. Ressler, J. Wong, M. Lovallo, M. Tsapatsis, Chem. Mater. 11 (1999) 3545.
[53] S. De Rossi, M.P. Casaletto, G. Ferraris, A. Cimino, G. Minelli, Appl. Catal. A 167 (1998) 257.
[54] B.M. Weckhuysen, I.E. Wachs, J. Phys. Chem. 100 (1996) 14437.